RSC Advances

PAPER

Cite this: *RSC Adv.*, 2023, **13**, 6909

Ag-embedded manganese oxide octahedral molecular sieve (Ag-OMS-2) nano-rods as efficient heterogeneous catalysts for hydration of nitriles to amides in aqueous solution†

Farimah Mazloom Kalimani and Alireza Khorshidi *

Received 15th January 2023
Accepted 23rd February 2023

DOI: 10.1039/d3ra00292f

rsc.li/rsc-advances

Silver-embedded manganese oxide octahedral molecular sieve (Ag-OMS-2) nano-rods were synthesized using a pre-incorporation approach, and unambiguously characterized by transmission electron microscopy (TEM), field emission scanning electron microscopy (FESEM), energy dispersive X-ray spectroscopy (EDS), X-ray diffraction (XRD), Fourier transform infrared spectroscopy (FTIR), X-ray photoelectron spectroscopy (XPS), and thermogravimetric analysis (TGA). A highly uniform distribution of Ag nanoparticles embedded in the porous structure of OMS-2, was found to be in favor of high catalytic activity of the composite for hydration of nitriles to corresponding amides in aqueous solution. By using a catalyst dosage of 30 mg per mmol of substrate, in the temperature range of 80–100 °C, and reaction times of 4–9 h, excellent yields (73–96%) of the desired amides (13 examples) were obtained. Also, the catalyst was easy to recycle, and showed a slight decrease in efficiency after six consecutive runs.

Introduction

One of the well-known classic reactions in the organic synthesis and chemical industries is hydration of nitriles to their corresponding amides. These are important structural units in the production of pharmaceuticals, plastics, fertilizers, detergents and lubricants.[1,2] Traditional catalytic systems were established by employing homogeneous strong acid and base catalysts. Nevertheless, these classic methods have some disadvantages, including over hydrolysis of amides into carboxylic acids, and generation of a massive amount of salts after neutralization of the catalysts.[3] It is well known that transition metals can enhance the rate of the hydration step *via* coordination with the CN bonds.[4] In this regard, there are some reports on the activation of nitriles by homogeneous transition-metal complexes including Cu,[5,6] Co,[7] Mo,[8] Rh,[9,10] and Ir.[11] However, these are associated with some drawbacks, including difficulties in the catalyst separation from the products, use of organic solvents, high cost of ligands, and complexity in recovery and reuse of the catalyst.[12–15] The growing interest in developing eco-friendly and practical methods for organic syntheses has drawn attention to heterogeneous transition-metal catalysts in aqueous medium under neutral conditions, which offers benefits such as high activity, ease of handling, and recovery.[16–19] In the past decades, several heterogeneous catalysts such as nanorod MnO_2, Ru/MnO_2, CeO_2, and Co_3O_4 have been shown to exhibit significant catalytic activity toward hydration of nitriles.[20–23] Single-atom catalysts (SACs) have received increasing attention in recent years due to having the advantages of both homogeneous and heterogeneous catalysts, such as isolated active sites, stability, and easy separation. This category of catalysts exposes good activity and selectivity in various oxidation, reduction, and coupling reactions.[24–26] Although water is an ideal solvent for the hydration of nitriles from environmental and practical points of view, a vast majority of the catalysts are reported in organic media or in the presence of only small amounts of water.[15,27–31] Therefore, development of environmentally benign and safe processes is still in the focus of attention. Due to salient features like multivalent Mn species (+2, +3, and +4), high surface area, porous structure, easy release of lattice oxygen, and cheapness, octahedral manganese oxide molecular sieve (cryptomelane, K-OMS-2)[32] has been widely used in heterogeneous catalysis,[33] energy storage,[34] sensors,[35] rechargeable batteries,[36] and wastewater treatment.[37–39] OMS-2 has a one-dimensional 0.46 nm × 0.46 nm tunnel structure, with MnO_6 octahedra as basic building units linked by edges or corners, to construct double MnO_6 chains.[40] Presence of K^+ ions and slight amounts of water molecules inside the tunnels, is necessary to balance the charge and support the structure.[41] Alkali or transition metal cations can be incorporated into the channels of OMS-2. These metal-modified OMS-2 samples have shown more reactive sites and improved catalytic properties.[42]

Department of Chemistry, Faculty of Sciences, University of Guilan, 41335-1914, Rasht, Iran. E-mail: khorshidi@guilan.ac.ir; Fax: +98-1333367262; Tel: +98-9113397159

† Electronic supplementary information (ESI) available. See DOI: https://doi.org/10.1039/d3ra00292f

Silver is a cheaper precious metal compared to other noble metals (Au and Pt) and has antimicrobial,[43–45] optical scattering,[46,47] and electrical conductivity[48,49] properties. In some cases, Ag has shown a better catalytic oxidation performance than common transition metal oxides.[41,50] Indeed, various researchers have studied the hydration of nitriles to amides by Ag NPs. Nevertheless, most of the reactions based on Ag catalysts, are associated with serious drawbacks including high reaction temperatures, need for an inert atmosphere, large amounts of Ag NPs, and catalyst recycling issues.[3,16,17,19,50,51] In order to improve the catalytic activity of cryptomelane, K^+ ions can be partially replaced by Ag^+ during the synthesis.[52] In this regard, Yadav *et al.*[53] reported the catalytic performance of Ag doped OMS-2 (Ag-OMS-2) for hydrogenation of nitrobenzene to aniline. The weak acidic and basic sites of the catalyst resulted in the stop of hydrogenation at the azobenzene stage as an intermediate product. Moreover, Dong *et al.*[54] prepared Ag-OMS-2 by various methods and studied the effect of preparation method on the oxidation of ethyl acetate and formaldehyde. Chen *et al.*[42] revealed the high catalytic performance of Ag-OMS-2 nanorods synthesized by a solid-state approach in CO oxidation, and attributed it to the enhanced oxygen activation and CO absorption in the presence of Ag^+ in the tunnel structure.

Herein, we report the Ag-embedded OMS-2 nano-rods as a high-performance catalyst for conversion of a broad range of nitriles (homo/hetero aromatic and aliphatic) to primary amides in water as a green solvent.

Experimental

Synthesis of Ag-OMS-2

Silver-embedded manganese oxide octahedral molecular sieve nano-rods (Ag-OMS-2) were prepared according to a previous report with minor modifications.[54] In a typical run, 3.66 mmol of silver nitrate was dissolved in a solution of 10.6 mmol of potassium permanganate in 25 mL of deionized water. Meanwhile, a second solution was prepared by adding 1.7 mL of concentrated nitric acid to a solution of 16.4 mmol of manganese sulfate in 8.5 mL of deionized water. The first solution was added dropwise to the second solution under vigorous stirring, and the resulting dark brown suspension was refluxed at 110 °C for 24 h. After filtration, the precipitate was washed with distilled water until neutral pH and dried at 120 °C for 12 h. Then the precipitate was dispersed in 25 mL of distilled water and treated with a freshly prepared solution of $NaBH_4$ (20 mL, 50 mM) for 1 h to ensure complete reduction of silver ions. Finally, the resulting Ag-OMS-2 was filtered and oven-dried at 100 °C overnight.

Hydration of nitriles

A round-bottomed flask was charged with Ag-OMS-2 (0.03 g), water (4.0 mL) and nitrile compound (1.0 mmol), and vigorously stirred at 90 °C for 4 h. After completion of the reaction (monitored by TLC (*n*-hexane : EtOAc 2 : 4)), the catalyst was separated by centrifugation and the solution was extracted with dichloromethane (3 × 5 mL). The collected organic phase was dried over anhydrous Na_2SO_4. The solvent was then evacuated by rotary evaporation and the resulting amides were characterized by ^{1}H-NMR spectra in comparison with authentic samples. Column chromatography on silica gel with dichloromethane as eluent was applied when appropriate.

Characterizations

Powder X-ray diffraction (XRD) patterns were recorded using a PANalytical X'Pert Pro MPD diffractometer with Cu Kα radiation ($\lambda = 0.15404$ nm). Surface morphology of the samples was observed by a scanning electron microscope (SEM) (MIRA3 TESCAN-XMU) equipped with EDX facilities. Transmission electron microscopy (TEM) was performed by using a Philips CM120 instrument. Fourier-transform infrared (FT-IR) spectra were recorded in the range of 400–4000 cm^{-1} on a Bruker Alpha spectrometer. Oxidation states of the catalyst elements were studied by X-ray photoelectron spectroscopy (XPS), using a Bestec spectrometer with an Al Kα X-ray anode source under a pressure of 10^{-10} mbar. The charging effect was calibrated by adjusting the binding energy of C 1s to 248.6 eV. Thermogravimetric analysis (TGA) was carried out by a TA SDT-Q600 device to study the thermal stability of the catalyst. The sample was heated from room temperature to 900 °C under flowing N_2 (ramp 10 °C min^{-1}).

Results and discussion

Characterization of the Ag-OMS-2

Fig. 1 compares the FTIR spectra of OMS-2 and Ag-OMS-2 samples. Both displayed characteristic bands of the Mn–O vibrations of octahedral MnO_6 species in the range of 400–800 cm^{-1}.[42,55] Replacement of K^+ with Ag^+ resulted in a slight change in the intensity and position of the band at 716 cm^{-1}, probably due to the Ag–O–Mn oxygen-bridged bond.[41] Also, the absorption band intensity at 1634 cm^{-1} increased compared to

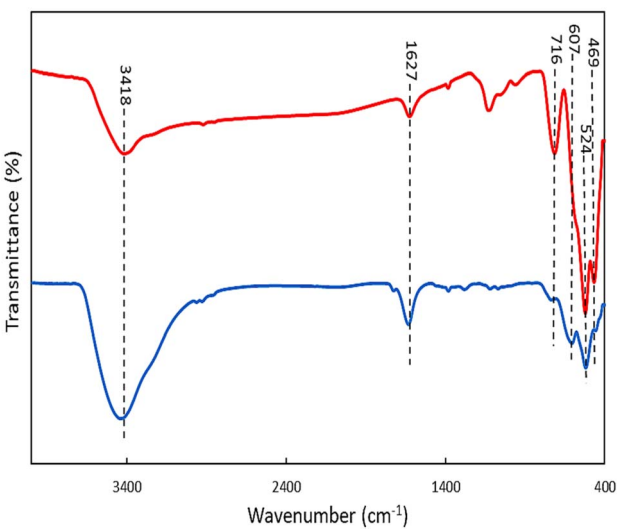

Fig. 1 FT-IR spectra of OMS-2 (up) and Ag-OMS-2 (bottom).

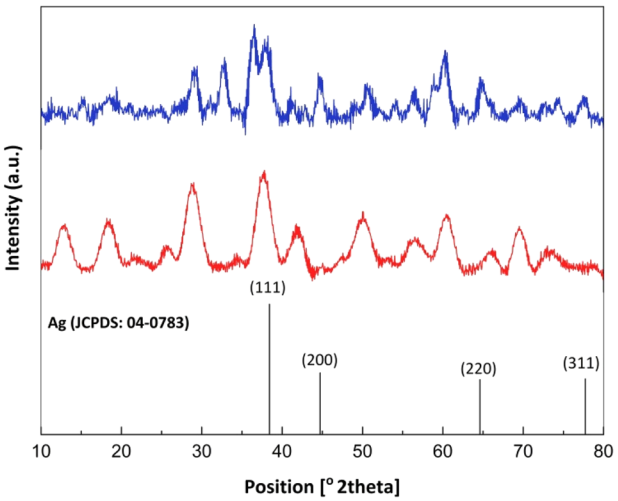

Fig. 2 XRD patterns of OMS-2 (up), Ag-OMS-2 (middle) and hexagonal Ag (JCPDS card no. 04-0783, bottom).

the undoped OMS-2, indicating that more hydroxyl groups were present in the structure, due to the increased surface defects and more sites to absorb water molecules.[56]

Fig. 2 shows the XRD patterns of the synthesized samples. The main diffraction peaks at 2θ 12.2, 17.9, 28.4, 37.2, 41.6, 49.5, and 59.9° corresponding to the (101), (002), (301), (211), (310), (114), and (600) crystal faces, are the characteristic peaks of K-OMS-2 (Fig. 2, middle, JCPDS card number 29-1020).[57] After incorporation of silver species, there was no significant change in the tunnel framework of OMS-2 nanorods, and diffraction peaks attributable to hexagonal phase of metallic Ag were appeared at 2θ 38.2, 44.7, 64.9, and 77.7° corresponding to the (111), (311), (220), and (200) planes) (JCPDS card number 04-783).[43] However, decrease in the intensity of the peaks in the XRD pattern of Ag-OMS-2 (Fig. 2, up) may address some structural changes upon reduction of Ag^+, despite the smaller size of Ag^+ (126 pm) compared to K^+ (138 pm).[33] The standard XRD pattern of Ag is also included for comparison (Fig. 2, bottom).[58]

Fig. 3 shows the FESEM image of OMS-2 (a), and FESEM and TEM images of Ag-OMS-2 (b). Both samples exhibited the typical morphology of cryptomelane nanorods. Ag-OMS-2 nanoparticles were appeared as needle-like nanorods ranging from 20 to 30 nm in diameter, and 100 to 300 nm in length. There were no significant structural defects compared to the unmodified OMS-2. The spherical particles ranging from 30 to 50 nm can be attributed to Mn_2O_3 or very large silver particles.[42,54] As a result of incorporation and *in situ* reduction of Ag^+ ions inside the tunnels of OMS-2, it is hard to capture the metallic Ag particles, even with TEM imaging (Fig. 3c).

The EDS mapping images of the constituent elements of Ag-OMS-2 including Ag, K, Mn, and O are shown in Fig. 4. Clearly, a uniform dispersion of Ag species in the sampled area is visible. Also, presence of K^+ in the modified sample indicates that potassium has not been completely substituted by Ag, and K^+ still co-exists in the catalyst structure.

Thermal stability of the K-OMS-2 and Ag-OMS-2 samples were also studied by using TGA technique in the temperature

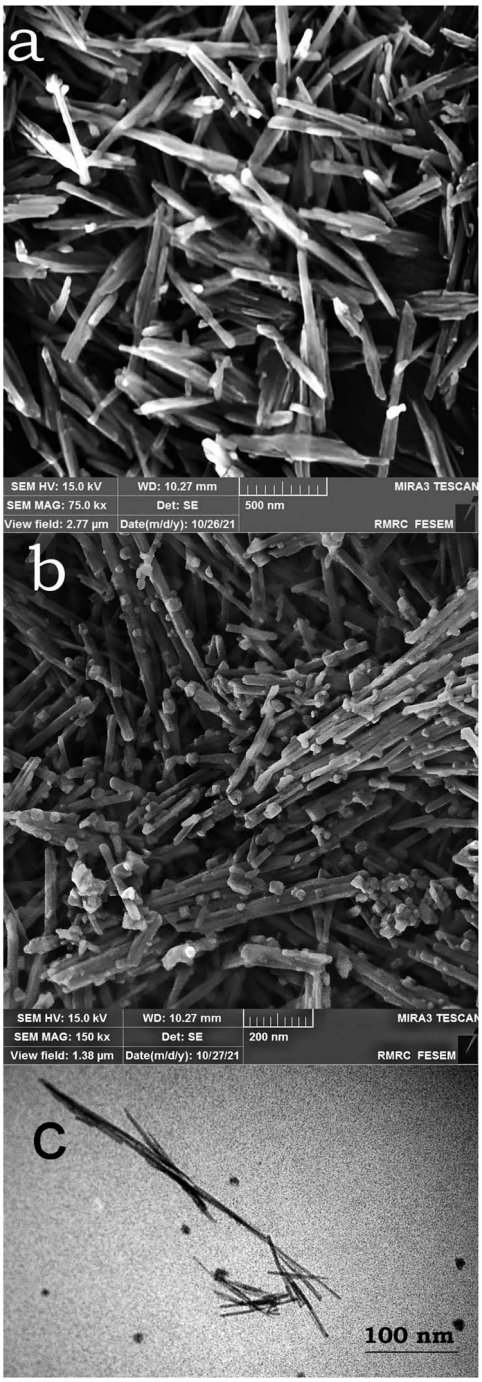

Fig. 3 FESEM image of OMS-2 (a), and FESEM and TEM images of Ag-OMS-2 (b and c).

range of 25–900 °C (Fig. 5). Probably, the first weight loss (~4%) occurred in the range of 100–300 °C is due to the removal of adsorbed water, carbon dioxide, and some physisorbed oxygen.[59,60] From the comparison of the two curves, it can be inferred that the amount of water adsorbed in the Ag-OMS-2 tunnels is more than that of the K-OMS-2, as is clearly visible in the first stage. The second gradual weight loss in the range of 300–450 °C is attributed to the chemically sorbed active oxygen species.[60,61] Also, a remarkable weight loss (~4.5%) in the range

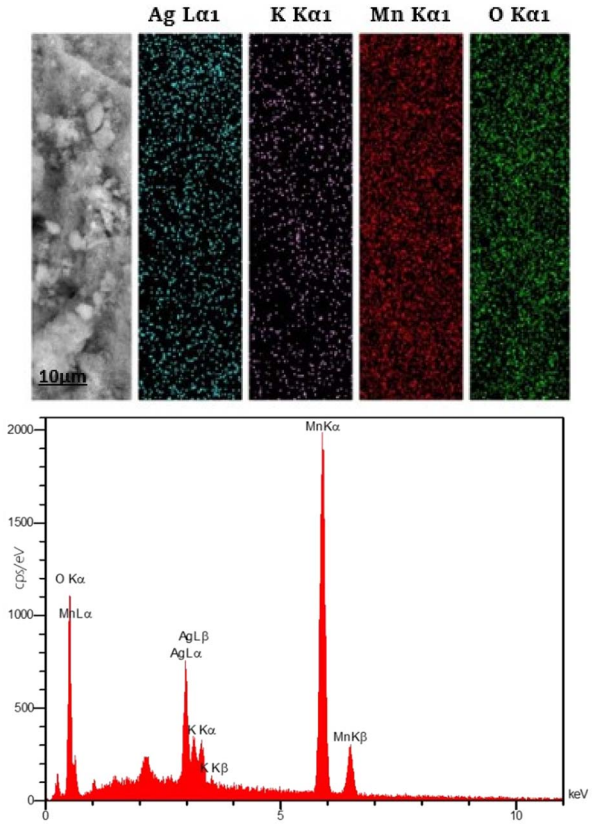

Fig. 4 Mapping analysis of Ag-OMS-2 (up), along with the corresponding EDSX analysis (bottom).

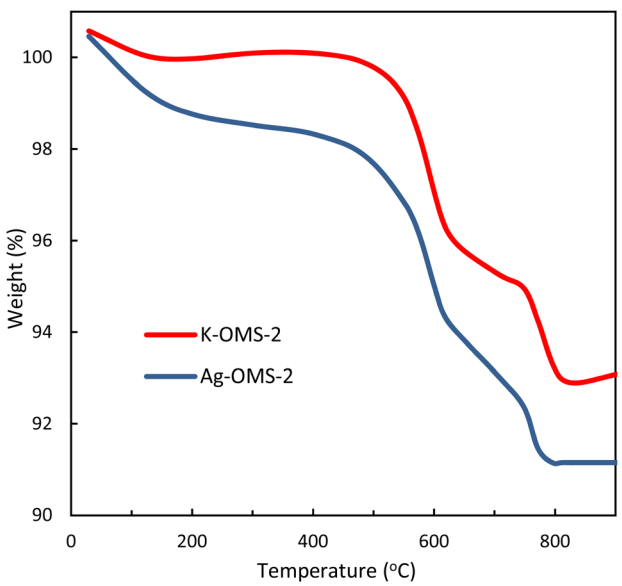

Fig. 5 TGA curves for OMS-2 and Ag-OMS-2.

of 450–650 °C is attributed to the evolution of the structural oxygen in the OMS-2 tunnel structure. The weight loss at temperatures above 650 °C can be attributed to the structural collapse of OMS-2.[56,62]

In order to clearly determine the oxidation state of silver in the Ag-OMS-2 sample, XPS analysis was performed. Fig. 6 shows the XPS spectrum of Ag-OMS-2, and clearly consists of the anticipated elements of O, Mn, Ag and K. As shown in Fig. 6b, the broad Mn $2p_{3/2}$ band exposes the spin–orbit splitting pair peaks at binding energies of 641.3 and 642.6 eV, which correspond to surface Mn^{3+} and Mn^{4+} species, respectively. The existence of mixed valence of Mn in the structure of OMS-2 causes electron transfer. Also, the Mn $2p_{1/2}$ peak located at BE = 654 eV is assignable to Mn^{3+}.[50] The molar ratio of Mn^{3+} to Mn^{4+} in Ag-OMS-2 was 2.84, calculated by CasaXPS software ver. 2.3.25. Fig. 6c shows the O 1s spectrum of the sample, which was fitted with two components. The peak at BE = 529.1 eV is attributed to the lattice oxygen (O_{latt}) and that at BE = 531 eV is attributed to the surface adsorbed oxygen (O_{ads}).[63] In the case of the Ag 3d XPS spectrum, two peaks located at the binding energies of 374.7 and 368.6 eV are ascribable to Ag $3d_{3/2}$ and Ag $3d_{5/2}$ states. These are in favour of the presence of silver as reduced Ag^0 species.[54]

Catalytic hydration of nitriles using Ag-OMS-2

Hydration of nitriles is one of the most important chemical processes to provide primary amides, which are important precursors in production of raw materials necessary for the chemical and pharmaceutical industries. In our study, hydration of benzonitrile to benzamide was selected as a model reaction to optimize the reaction conditions including temperature, catalyst loading, choice of solvent and reaction time. Initially, it was found that the amount of the catalyst has an important effect on the reaction yield. Increasing the amount of the catalyst from 10 to 30 mg, drastically increased the yield, due to the increase of the available active sites for the substrates to be converted. In the absence of the catalyst, however, no reaction occurred under the abovementioned conditions (Table 1, entries 1–5). When the reaction was carried out in presence of K-OMS-2 as catalyst, the product yield was negligible. This demonstrates a synergistic effect between silver nanoparticles and OMS-2 support (Table 1, entry 6). With regard to the solvent type, it was found that water is the best choice in terms of the reaction time and yield. Fortunately, this is in favour of the green chemistry principals. Protic solvents, including ethanol and methanol, resulted in lower yields than expected, even in companion with water (Table 1, entries 7–10). Aprotic solvents, such as toluene and THF, on the other hand, led to a further decrease in the reaction efficiency (Table 1, entries 11 and 12). It was also found that the reaction is very time consuming, even in presence of the Ag-OMS-2 catalyst. However, the conversion was increased upon elevation of temperature, and a maximum yield of 93% was obtained at 80 °C. Higher temperatures, on the other hand, had no significant positive effect on the reaction yield (Table 1, entries 13–16).

To study the generality and scope of the reaction, Ag-OMS-2 was applied to a wide range of nitriles (Table 2). Benzonitrile derivatives with electron-withdrawing (Table 2, entries 2–7) or electron-donating groups (Table 2, entries 8 and 9) exhibited comparable reactivity in terms of yield of the final product.

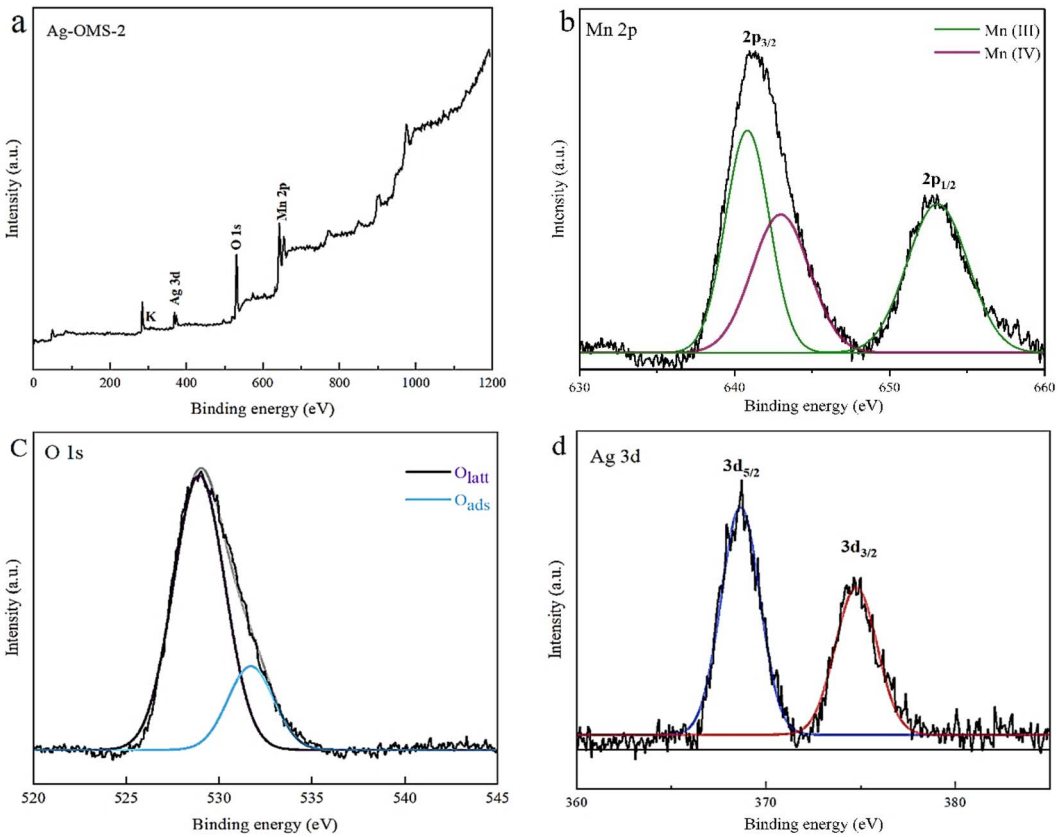

Fig. 6 XPS survey scan for the Ag-OMS-2 (a), Mn 2p (b), O 1s (c), and Ag 3d (d).

Electron-withdrawing substituents, however, resulted in slightly more yields as a result of making the nitrile carbon more susceptible to nucleophilic attack by an activated water molecule.[64] As expected, *ortho*-substituted benzonitriles produced lower yields than *meta*- and *para*-substituted analogues (Table 2, entries 2–4), probably due to the steric hindrance effects. Aliphatic substrates such as acetonitrile and acrylonitrile, on the other hand (Table 2, entries 10 and 11), required more times

Table 1 Optimization of the reaction conditions for the synthesis of benzamide from benzonitrile in presence of Ag-OMS-2 as catalyst[a]

Entry	Solvent	Catalyst amount[b] (mg)	Temperature (°C)	Time (h)	Yield (%)
1	Water	0	80	4	N.R.
2	Water	10	80	4	15
3	Water	20	80	4	68
4	Water	30	80	4	93
5	Water	40	80	4	96
6[c]	Water	30	80	4	Trace
7	Methanol	30	80	4	N.R.
8	Ethanol	30	80	4	20
9	Methanol : water (1 : 1)	30	80	4	48
10	Methanol : water (1 : 2)	30	80	4	70
11	Toluene	30	80	4	Trace
12	THF	30	80	4	Trace
13	Water	30	25	4	11
14	Water	30	40	4	28
15	Water	30	60	4	66
16	Water	30	100	4	95
17	Water	30	80	1	20
18	Water	30	80	2	42
19	Water	30	80	3	70

[a] Reaction conditions: Ag-OMS-2 as catalyst, solvent (4.0 mL), benzonitrile (1.0 mmol). [b] 4.87 mol% of Ag. [c] K-OMS-2 was used as catalyst.

Table 2 Hydration of diverse nitriles catalysed by Ag-OMS-2[a]

Entry	Substrate	Product	Temp. (°C)	Time (h)	Isolated yield (%)
1		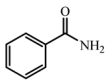	80	4	93
2	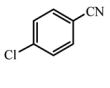	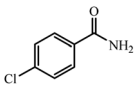	80	4	95
3	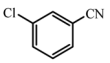	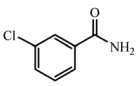	80	4	91
4		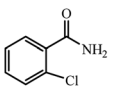	80	4	89
5	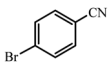	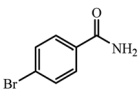	80	4	92
6	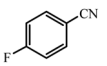	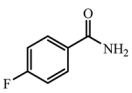	80	4	97
7	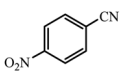	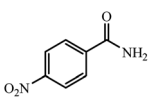	80	4	96
8	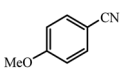	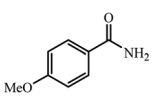	80	4	88
9	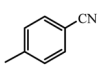	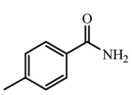	80	4	90
10	CH_3CN		100	9	70
11		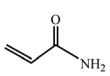	100	9	73
12		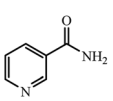	80	4	95
13		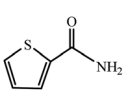	80	4	92

[a] Reaction conditions: nitrile (1.0 mmol), Ag-OMS-2 (30 mg), H_2O (4 mL), 80 °C. The products were isolated by either recrystallization or column chromatography, and confirmed by ^1H NMR.

and temperatures to convert to corresponding amides due to the increased electron density of nitrile carbon compared to aromatic nitriles. Heterocyclic amides are also an important class of mediators in medicinal chemistry. For example, nicotinamide is a form of vitamin B_3 and is used as a food and drug supplement in treating pellagra and skin inflammations.[65] Nevertheless, hydration of their nitrile precursors is somehow difficult as a result of the strong tendency of nitrile substrates toward metal centres.[66] Interestingly, our devised protocol resulted in excellent conversion of heteroaromatic nitriles containing S and N heteroatoms to their corresponding amides in a rather short time (Table 2, entries 12 and 13). According to these results, Ag-OMS-2 can be considered as an appropriate catalyst for the hydration of nitriles. It should be noted that, previous reports on Ag NPs as catalyst for the title reaction, require high temperatures (up to 140 °C) and large amounts of silver metal.

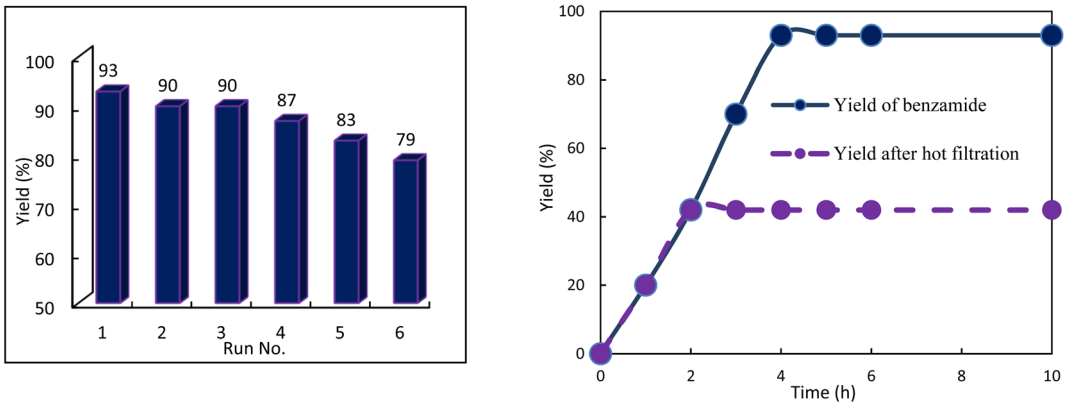

Fig. 7 (Left) Reusability of the Ag-OMS-2 for hydration of benzonitrile. (Right) The yield of benzamide in presence of Ag-OMS-2, and after its removal halfway.

Recovery and reuse of the Ag-OMS-2 catalyst was also tested. After each run, the filtered catalyst was Soxhlet-extracted with methanol for 1 h, and then oven-dried for 3 h. After six consecutive cycles, a reasonable decrease in efficiency of the catalyst was observed (Fig. 7). A hot filtration test was performed to investigate the leaching of silver from the OMS-2 support into the solution.

The experiment was carried out for the hydration of benzonitrile, and the catalyst was removed from the reaction liquor 2 h after the start of the reaction at 80 °C. The filtered solution was allowed to react until the end of the period (4 h) and no change in the product yield was observed during the last 2 h (Fig. 7). ICP analysis of the supernatant also confirmed the absence of silver ions. Thus, it can be concluded that silver was not leached out during the hydration reaction.

In addition, FESEM and TEM images of the catalyst recovered after the 6th run are presented in Fig. 8. As can be seen, the catalyst retained its morphology and structure.

A possible reaction mechanism for nitrile hydration over the Ag-OMS-2 is proposed in Fig. 9. Initially, nitrile is coordinated through the interaction of nitrogen with the surface of Ag NPs, as they carry a positive surface charge.[50] The active oxygen sites belonging to the OMS-2 structure (as Brønsted bases) effectively activate water molecules *via* Mn···O–H–OH interactions to form the $OH^{\delta-}$ species (step 1). Nucleophilic addition of hydroxyl to the nitrile leads to the formation of a negatively charged transition state (steps 2 and 3). After hydrogen abstraction from Mn–O···H by nitrogen, active oxygen sites regenerate on the metal oxide. Finally, the resulting hydrated nitrile species exchange ligand with the solvent, and amide is produced (step 4).

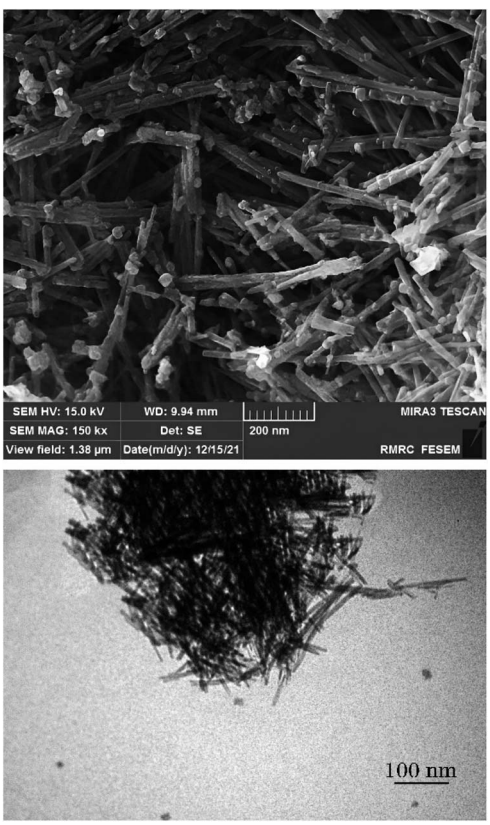

Fig. 8 FESEM (top) and TEM (bottom) images of the recovered catalyst after the 6th run.

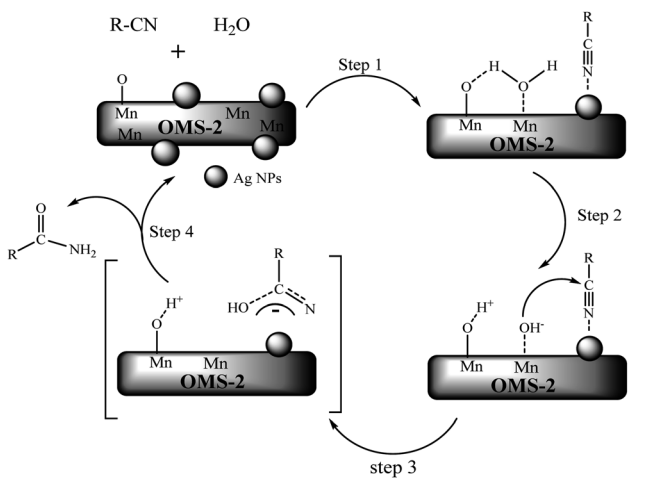

Fig. 9 A possible mechanistic pathway for Ag-OMS-2 catalysed hydration of nitriles.

Table 3 Comparison of the catalytic activity of Ag-OMS-2 with other systems reported for hydration of nitriles

Entry	Catalyst	Reaction conditions	Catalyst loading[a]	Yield (%)	Ref.
1	[(IPr)Au(NTf$_2$)]	H_2O : THF (1 : 1), 140 °C, MW, 2 h	2 mol%	99	15
2	Ag NPs@mPMF	H_2O, 90 °C, in air, 7 h	5 mol%	97	64
3	Ag–PAAS	H_2O, 90 °C, in air, 9 h	3 mol%	90	67
4	Ag/Fe_3O_4	H_2O, 150 °C, 6 h	3 mol%	99	68
5	Ag-CIN-1	H_2O, 100 °C, 3 h	50 mg	96	2
6	Ni NPs/HT	H_2O, 120 °C, 10 h	50 mg	85	69
7	Activated clay/C@Fe_2O_3	H_2O, KOH, 60 °C, 4 h	25 mg	81	70
8	[$RuH_2(PPh_3)_4$]	H_2O, 100 °C, 24 h	5 mol%	62	71
9	Ni(II) complex	H_2O, ^{i}PrOH, 70 °C, 6 h	2–10 mol%	91	29
10	Ru/chitin	H_2O, N_2 atmosphere, 120 °C, 20 h	2.3 mol%	97	72
11	Ag/SiO_2	H_2O, 140 °C, 3 h	45 mg	98	3
12	Ag-OMS-2	H_2O, 80 °C, 4 h	4.87 mol%	93	This work

[a] Mol% of the active ingredient relative to the nitrile substrate.

Table 3 compares our results with some of the other catalytic systems reported for hydration of nitriles. Some of these systems have serious limitations such as need for additives, use of organic solvents, prolonged reaction times, elevated temperatures, high loads of catalyst, and need for a neutral atmosphere.

Conclusions

Hydration of a broad range of nitriles to their corresponding amides was achieved by using Ag-OMS-2 nanoparticles as a heterogeneous catalyst under neutral conditions in water. According to the proposed mechanism, the observed efficiency can be attributed to the synergistic effect of silver with OMS-2 scaffold. Highlights of the present protocol include thermal stability of the catalyst, ease of catalyst recycling and work-up, and eco-friendly nature of the process as a result of using water as both a solvent and a hydrating agent.

Characterization data for the amide products

Benzamide.

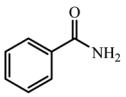

93% yield (112.6 mg); white solid; mp 124–126 °C; IR (KBr, cm^{-1}): 3371, 3173, 1660, 1576, 1501, 1403, 1184, 1120, 786, 634; ^{1}H NMR (250 MHz, $CDCl_3$): δ 7.79 (d, J = 7.76 Hz, 2H), 7.40–7.51 (m, 1H), 7.25 (s, 2H), 6.27 (s, NH, 2H).

4-Chlorobenzamide.

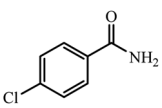

95% yield (147.8 mg); white solid; mp 179–181 °C; IR (KBr, cm^{-1}): 3431, 3280, 1656, 1626, 1410, 1346, 1203, 1092, 791, 697; ^{1}H NMR (250 MHz, $CDCl_3$): δ 7.73 (d, J = 6.5 Hz, 2H), 7.41 (d, J = 5.75 Hz, 2H), 5.80 (br, NH, 2H, exchange with solvent).

3-Chlorobenzamide.

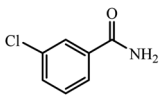

91% yield (141.5 mg); white solid; mp 132–133 °C; IR (KBr, cm^{-1}): 3355, 3199, 1676, 1616, 1435, 1325, 1302, 1102, 775; ^{1}H NMR (250 MHz, $CDCl_3$): δ 8.18 (s, 1H), 7.77–7.80 (d, J = 7.5 Hz, 1H), 7.58–7.63 (d, J = 12.5 Hz, 1H), 7.18–7.21 (t, J = 2.5 Hz, 1H), 5.88 (s, 2H).

2-Chlorobenzamide.

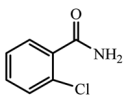

89% yield (138.4 mg); white solid; mp 142–145 °C; IR (KBr, cm^{-1}): 3392, 3198, 1645, 1620, 1460, 1403, 1216, 1119, 839, 768, 634; ^{1}H NMR (250 MHz, $CDCl_3$): δ 8.09 (d, J = 15.5 Hz, 1H), 7.46–7.54 (m, 1H), 7.09–7.30 (m, 1H), 6.68 (s, 1H), 6.17 (s, NH, 1H).

4-Bromobenzamide.

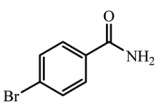

92% yield (184 mg); white solid; mp 192–193 °C; IR (KBr, cm^{-1}): 3352, 3164, 1654, 1620, 1407, 1279, 1014, 792; ^{1}H NMR (250 MHz, $CDCl_3$): δ 7.87 (d, J = 7.5 Hz, 2H), 7.67 (d, J = 4.25 Hz, 2H), 6.05 (br, NH, 2H, exchange with solvent).

4-Fluorobenzamide.

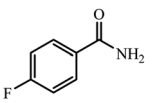

97% yield (134.9 mg); white solid; mp 155–157 °C; IR (KBr, cm^{-1}): 3335, 3169, 2932, 1666, 1618, 1405, 1215, 1112, 780; ^{1}H NMR (250 MHz, $CDCl_3$): δ 7.83 (t, J = 4.25 Hz, 2H), 7.11–7.21 (m, 2H), 6.06 (s, NH, 2H).

4-Nitrobenzamide.

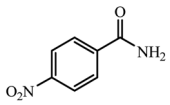

96% yield (159.4 mg); yellow solid; mp 197–199 °C; IR (KBr, cm^{-1}): 3474, 3350, 3166, 1676, 1599, 1524, 1410, 1344, 1139, 1111, 1007, 864, 763, 707, 658, 607; ^{1}H NMR (250 MHz, $CDCl_3$) δ 8.30 (d, $J = 8.28$ Hz, 2H), 7.96 (d, $J = 8.25$ Hz, 2H), 7.26 (br, NH, 2H, exchange with solvent).

4-Methoxybenzamide.

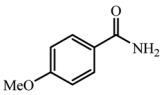

88% yield (133 mg); white solid; mp 166–167 °C; IR (KBr, cm^{-1}): 3391, 3169, 1647, 1615, 1571, 1423, 1393, 1251, 1180, 1023, 850, 811, 649; ^{1}H NMR (250 MHz, $CDCl_3$): δ 7.76 (d, $J = 7.0$ Hz, 2H), 6.91 (d, $J = 7.0$ Hz, 2H), 5.92 (s, NH, 2H), 3.84 (s, 3H).

4-Methylbenzamide.

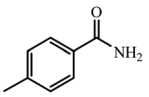

90% yield (121.6 mg); white solid; mp 157–159 °C; IR (KBr, cm^{-1}): 3343, 3165, 1671, 1616, 1568, 1412, 1287, 1119, 840, 793, 672; ^{1}H NMR (250 MHz, $CDCl_3$): δ 7.69 (d, $J = 7.75$ Hz, 2H), 7.23 (d, $J = 7.75$ Hz, 2H), 5.96 (br, NH, 2H, exchange with solvent), 2.40 (s, 3H).

Acetamide.

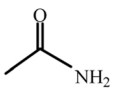

70% yield (41.3 mg); white solid; mp 79–80 °C; IR (KBr, cm^{-1}): 3512, 3323, 2962, 1369, 1109, 996, 813, 644; ^{1}H NMR (250 MHz, DMSO-d_6): δ 6.60 (s, 2H), 1.73 (s, 3H).

Acrylamide.

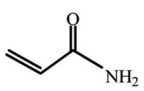

73% yield (51.8 mg); white solid; mp 84–87 °C; IR (KBr, cm^{-1}): 3466, 3355, 2864, 2337, 1629, 1509, 1390, 1107, 1021, 1135, 711; ^{1}H NMR (250 MHz, DMSO-d_6): δ 6.15–6.79 (m, 2H), 5.34 (s, NH, 2H).

Nicotinamide.

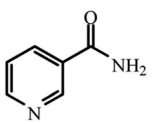

95% yield (116 mg); white solid; mp 126–128 °C; IR (KBr, cm^{-1}): 3354, 3156, 2915, 1666, 1606, 1399, 1192, 1089, 607; ^{1}H NMR (250 MHz, DMSO-d_6): δ 9.07 (d, $J = 12.5$ Hz, 1H), 8.60–8.70 (m, 1H), 8.14–8.28 (m, 1H), 7.58 (s, 1H), 7.28–7.34 (m, 1H).

Thiophene-2-carboxamide.

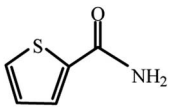

92% yield (116.9 mg); yellow solid; mp 176–178 °C; IR (KBr, cm^{-1}): 3304, 3078, 1612, 1538, 1404, 1345, 1278, 1228, 1086, 931, 832, 689; ^{1}H NMR (250 MHz, $CDCl_3$): δ 7.84 (t, $J = 5.5$ Hz, 1H), 7.57 (d, $J = 7.0$ Hz, 1H), 7.14 (t, $J = 7.0$ Hz, 1H), 5.66 (br, 2H, exchange with solvent).

Conflicts of interest

There are no conflicts to declare.

Acknowledgements

Partial support of this study by Research Council of University of Guilan is gratefully acknowledged.

References

1 N. S. Thirukovela, R. Balaboina, S. Kankala, R. Vadde and C. S. Vasam, *Tetrahedron*, 2019, **75**, 2637–2641.
2 N. Salam, S. K. Kundu, R. A. Molla, P. Mondal, A. Bhaumik and S. M. Islam, *RSC Adv.*, 2014, **4**, 47593–47604.
3 K. I. Shimizu, N. Imaiida, K. Sawabe and A. Satsuma, *Appl. Catal., A*, 2012, **421–422**, 114–120.
4 V. Cadierno, J. Francos and J. Gimeno, *Chem.–Eur. J.*, 2008, **14**, 6601–6605.
5 A. Ishizuka, Y. Nakazaki and T. Oshiki, *Chem. Lett.*, 2009, **38**, 360–361.
6 T. J. Ahmed, S. M. M. Knapp and D. R. Tyler, *Coord. Chem. Rev.*, 2011, **255**, 949–974.
7 J. H. Kim, J. Britten and J. Chin, *J. Am. Chem. Soc.*, 1993, **115**, 3618–3622.
8 K. L. Breno, M. D. Pluth and D. R. Tyler, *Organometallics*, 2003, **22**, 1203–1211.
9 A. Goto, K. Endo and S. Saito, *Angew. Chem., Int. Ed.*, 2008, **47**, 3607–3609.
10 M. C. K. B. Djoman and A. N. Ajjou, *Tetrahedron Lett.*, 2000, **41**, 4845–4849.
11 H. Takaya, K. Yoshida, K. Isozaki, H. Terai and S. I. Murahashi, *Angew. Chem., Int. Ed.*, 2003, **42**, 3302–3304.
12 Í. Ferrer, J. Rich, X. Fontrodona, M. Rodríguez and I. Romero, *Dalton Trans.*, 2013, **42**, 13461–13469.
13 E. Tomás-Mendivil, F. J. Suárez, J. Díeza and V. Cadierno, *Chem. Commun.*, 2014, **50**, 9661–9664.
14 P. Crochet and V. Cadierno, *Dalton Trans.*, 2014, **43**, 12447–12462.
15 R. S. Ramón, N. Marion and S. P. Nolan, *Chem.–Eur. J.*, 2009, **15**, 8695–8697.
16 T. Mitsudome, *et al.*, *Chem. Commun.*, 2009, 3258–3260.

17 E. L. Downs and D. R. Tyler, *Coord. Chem. Rev.*, 2014, **280**, 28–37.
18 S. Kumar and P. Das, *New J. Chem.*, 2013, **37**, 2987–2990.
19 A. Y. Kim, H. S. Bae, S. Park, S. Park and K. H. Park, *Catal. Lett.*, 2011, **141**, 685–690.
20 H. Wang, *et al.*, *Ind. Eng. Chem. Res.*, 2019, **58**, 17319–17324.
21 M. A. Hussain, *et al.*, *J. Ind. Eng. Chem.*, 2021, **99**, 187–195.
22 M. Tamura, A. Satsuma and K. I. Shimizu, *Catal. Sci. Technol.*, 2013, **3**, 1386–1393.
23 Y. Gangarajula and B. Gopal, *Chem. Lett.*, 2012, **41**, 101–103.
24 S. Ding, M. J. Hülsey, H. An, Q. He, H. Asakura, M. Gao and N. Yan, *CCS Chem.*, 2021, **10**, 1814–1822.
25 M. J. Hülsey, S. Baskaran, S. Ding, S. Wang, H. Asakura, S. Furukawa and N. Yan, *CCS Chem.*, 2022, **10**, 3296–3308.
26 M. J. Hülsey, V. Fung, X. Hou, J. Wu and N. Yan, *Angew. Chem.*, 2022, **40**, e202208237.
27 S. I. Murahashi, S. Sasao, E. Saito and T. Naota, *Tetrahedron*, 1993, **39**, 8805–8826.
28 S. Murahashi, S. Sasao, E. Saito and T. Naota, *J. Org. Chem.*, 1992, **9**, 2521–2523.
29 K. Singh, A. Sarbajna, I. Dutta, P. Pandey and J. K. Bera, *Chem.–Eur. J.*, 2017, **23**, 7761–7771.
30 T. Oshiki, H. Yamashita, K. Sawada, M. Utsunomiya, K. Takahashi and K. Takai, *Organometallics*, 2005, **26**, 6287–6290.
31 E. S. Kim, H. S. Kim and J. N. Kim, *Tetrahedron Lett.*, 2009, **24**, 2973–2975.
32 A. Iyer, H. Galindo, S. Sithambaram, C. King'ondu, C. H. Chen and S. L. Suib, *Appl. Catal., A*, 2010, **375**, 295–302.
33 S. Sithambaram, R. Kumar, Y. C. Son and S. L. Suib, *J. Catal.*, 2008, **253**, 269–277.
34 S. Rasul, S. Suzuki, S. Yamaguchi and M. Miyayama, *Electrochim. Acta*, 2013, **110**, 247–252.
35 M. Nogami, T. Maeda and T. Uma, *Sens. Actuators, B*, 2009, **137**, 603–607.
36 H. Zhang, *et al.*, *ACS Sustainable Chem. Eng.*, 2017, **5**, 6727–6735.
37 W. Hou, S. Wang, X. Bi, X. Meng, P. Zhao and X. Liu, *Chin. Chem. Lett.*, 2021, **32**, 2513–2518.
38 M. Yao, M. Xie, S. Zhang, J. Yuan, L. Zhao and R. S. Zhao, *Sep. Purif. Technol.*, 2022, **302**, 122145.
39 P. Ye, Q. Zou, L. An, Y. Wei, A. Xu and X. Li, *J. Colloid Interface Sci.*, 2019, **535**, 481–490.
40 S. L. Suib, *J. Mater. Chem.*, 2008, **18**, 1623–1631.
41 J. Fu, N. Dong, Q. Ye, S. Cheng, T. Kang and H. Dai, *New J. Chem.*, 2018, **42**, 18117–18127.
42 J. Chen, J. Li, H. Li, X. Huang and W. Shen, *Microporous Mesoporous Mater.*, 2008, **116**, 586–592.
43 S. K. Kailasa, T. J. Park, J. V. Rohit and J. R. Koduru, *Nanopart. Pharmacother.*, 2019, 461–484.
44 V. K. Sharma, R. A. Yngard and Y. Lin, *Adv. Colloid Interface Sci.*, 2009, **1–2**, 83–96.
45 N. Durán, M. Durán, M. B. De Jesus, A. B. Seabra, W. J. Fávaro and G. Nakazato, *Nanomedicine*, 2016, **3**, 789–799.
46 D. D. Evanoff Jr and G. Chumanov, *ChemPhysChem*, 2005, **7**, 1221–1231.
47 I. A. Wani, S. Khatoon, A. Ganguly, J. Ahmed, A. K. Ganguli and T. Ahmad, *Mater. Res. Bull.*, 2010, **8**, 1033–1038.
48 P. C. Ma, B. Z. Tang and J. K. Kim, *Carbon*, 2008, **11**, 1497–1505.
49 H. Wei and H. Eilers, *Thin Solid Films*, 2008, **2**, 575–581.
50 J. Liu, L. Ke, L. Sun, F. Pan, X. Yuan and D. Xia, *J. Environ. Chem. Eng.*, 2021, **9**, 106199.
51 K. Kawai, H. Kawakami, T. Narushima and T. Yonezawa, *J. Nanopart. Res.*, 2015, **17**, 1–9.
52 M. Özacar, A. S. Poyraz, H. C. Genuino, C. H. Kuo, Y. Meng and S. L. Suib, *Appl. Catal., A*, 2013, **462–463**, 64–74.
53 G. D. Yadav and R. K. Mewada, *Chem. Eng. J.*, 2013, **221**, 500–511.
54 N. Dong, J. Fu, Q. Ye, M. Chen, Z. Fu and H. Dai, *Catal. Surv. Asia*, 2020, **24**, 259–268.
55 C. M. Julien, M. Massot and C. Poinsignon, *Spectrochim. Acta, Part A*, 2004, **60**, 689–700.
56 J. Xu, J. Li, Q. Yang, Y. Xiong and C. Chen, *Electrochim. Acta*, 2017, **251**, 672–680.
57 N. Dong, M. Chen, Q. Ye, D. Zhang and H. Dai, *J. Environ. Sci.*, 2022, **112**, 258–268.
58 S. Ansari, A. Khorshidi and S. Shariati, *RSC Adv.*, 2020, **10**, 3554–3565.
59 R. Wang and J. Li, *Environ. Sci. Technol.*, 2010, **11**, 4282–4287.
60 J. Li, R. Wang and J. Hao, *J. Phys. Chem. C*, 2010, **23**, 10544–10550.
61 G. Qiu, H. Huang, S. Dharmarathna, E. Benbow, L. Stafford and S. L. Suib, *Chem. Mater.*, 2011, **17**, 3892–3901.
62 H. Sun, S. Chen, P. Wang and X. Quan, *Chem. Eng. J.*, 2011, **178**, 191–196.
63 F. Gao, X. Tang, H. Yi, C. Chu, N. Li, J. Li and S. Zhao, *Chem. Eng. J.*, 2017, **322**, 525–537.
64 K. Ghosh, A. Iqubal, R. A. Molla, A. Mishra and S. M. Islam, *Catal. Sci. Technol.*, 2015, **5**, 1606–1622.
65 S. C. Roy, P. Dutta, L. N. Nandy, S. K. Roy, P. Samuel, S. M. Pillai and M. Ravindranathan, *Appl. Catal., A*, 2005, **290**, 175–180.
66 *Silver Nanoparticles*, ed. D. Pozo Perez, In-Teh Olajnica 19/2, 32000 Vukovar, Croatia, 2010.
67 J. Li, G. Tang, Y. Wang, Y. Wang, Z. Li and H. Li, *New J. Chem.*, 2016, **40**, 358–364.
68 H. Woo, K. Lee, S. Park and K. H. Park, *Molecules*, 2014, **19**, 699–712.
69 T. Subramanian and K. Pitchumani, *Catal. Commun.*, 2012, **29**, 109–113.
70 T. Rahman, G. Borah and P. K. Gogoi, *J. Chem. Sci.*, 2021, **133**, 20–22.
71 R. García-Álvarez, J. Francos, E. Tomás-Mendivil, P. Crochet and V. Cadierno, *J. Organomet. Chem.*, 2014, **771**, 93–104.
72 A. Matsuoka, *et al.*, *RSC Adv.*, 2015, **5**, 12152–12160.